Isolated Matrix Converter for Interconnection of Low Voltage AC Grids to DC Grids

Bárbara Miguel Machado Cosme
barbara.cosme@tecnico.ulisboa.pt

Instituto Superior Técnico, Lisboa, Portugal

January 2021

Abstract

The purpose of this paper is to develop an isolated and bidirectional AC/DC matrix converter, to connect an AC grid to a DC grid. By using this converter, it will be possible to reduce the losses of today's AC network and make it more efficient by reducing the conversion levels that currently exist. The proposed system is composed of two matrix converters, a High-Frequency Transformer, and a DC/DC step-up converter. The inclusion of this converter must ensure that disturbances in both networks are minimal, so a non-linear control system for DC grid voltage is developed, based on Lyapunov's stability theory. Finally, Matlab's Simulink tool is used, and the system is simulated in several different scenarios. Through these simulations, it is possible to demonstrate that the system is bidirectional and that in all cases, the control system works correctly.

Keywords: AC/DC hybrid network, AC/DC matrix converter, Bidirectional, High-Frequency Transformer, Non-linear controller.

1. Introduction

Since the end of the famous "War of Currents" from around 1891 that AC systems developed and expanded very quickly into a centralized, radial system, as shown in the leftmost diagram of figure 1 [1]. However, technological advances and the inclusion of new elements in the network lead to rethinking whether the present architecture is still adequate or not. [1].

Over the years, there has been an evolution in the typology of loads. Conventional AC loads, such as some home appliances, are gradually changing and instead of having only one AC motor, they are also starting to include an AC/DC converter to minimize consumption and consequently save energy [1, 2]. Furthermore, in our daily life, we are increasingly surrounded by DC loads, whether at home, in the office, or on the street, which leads to the need to include AC/DC converters to connect these loads to the AC grid [2, 3].

In recent years, there has been an increase in renewable energy sources, which has made the system decentralized and the power flow in the distribution network is now bidirectional, as presented in the second diagram of figure 1 [1]. Besides, some of these sources are operated in DC or have a DC intermediate link, so they can be directly connected to a DC grid [1, 2, 3]. It then appears that the inclusion of renewable sources and the change in load typology has increased system losses due to the need to include several AC/DC or DC/AC converters [1]. Therefore, this paper proposes an isolated and bidirectional AC/DC matrix converter, that allows connecting a low voltage single-phase AC grid to a DC grid, as presented in figure 2. Consequently, it is possible to reduce the number of converters, increasing the overall efficiency of the system. The proposed system is composed of two matrix converters, a High-Frequency Transformer (HFT), and a DC/DC step-up converter.

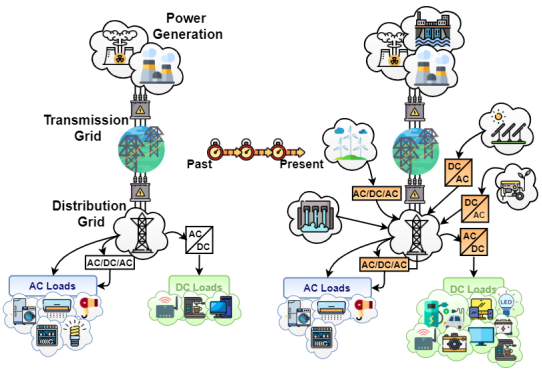

Figure 1: Evolution of network architecture (based from [1] and the icons are from [4]).

The paper, besides presenting all the elements of the system and performing their sizing, also pro-

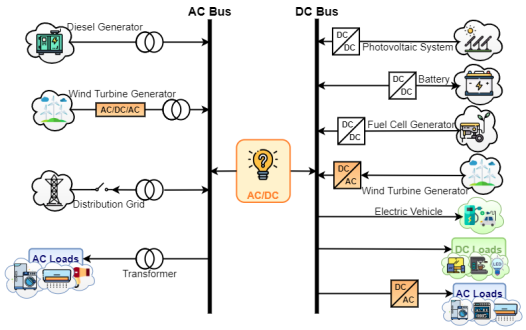

Figure 2: Solution proposed: an AC/DC hybrid system (based from [1, 3] and the icons are from [4]).

poses a non-linear control system to ensure that the disturbances caused by the conversion system are minimal.

This paper is organized as follows: this section is the introduction. In section 2, the model of the bidirectional and isolated AC/DC matrix converter is presented, which includes a detailed study of the proposed system, and the sizing of its filters. In section 3, a non-linear control system based on the backstepping and sliding mode control theories is presented. In section 4, the simulation results are presented considering different scenarios. In section 5, the conclusions of the work accomplished are presented.

2. Proposed Solution

Selecting an appropriate typology for a converter is crucial to achieving all the proposed requirements [5]. Figure 3 presents the conversion system proposed in this article, which aims to connect a single phase of the low voltage AC grid to a DC grid.

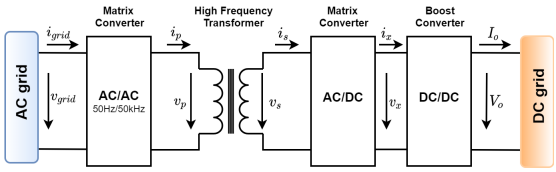

Figure 3: Proposed system diagram.

The elements that form the system are an AC/AC matrix converter that has the purpose of increase the frequency of the AC grid voltage to the switching frequency of the system, an HFT that ensures galvanic isolation, and also an AC/DC matrix converter and a DC/DC elevator converter, which together have the function of converting the high frequency AC voltage into a DC voltage.

2.1. High-Frequency Transformer

Since the introduction of AC systems in 1887, the magnetically coupled transformer has become an essential asset in the electrical grid [6]. Besides, technological advances in recent years have allowed the development of power electronic converters and the improvement of semiconductor technology [7]. As a result, multi-functional equipment has been created for applications in low voltage networks [7]. Therefore, the HFT is expected to be able to replace the conventional 50/60 Hz transformer [7].

The HFT generally has a work frequency range from several kilohertz to hundreds of kilohertz and, compared to the conventional 50/60 Hz transformer, has more advantages [8]. Because besides being galvanically insulated and having the capacity to reduce/increase the voltage value, it also allows intelligent energy management, power quality enhancement, low weight, low volume, and high energy density [9, 10, 11].

2.2. Matrix Converter

The name "Matrix Converter" (MC) appeared in 1980, when Venturini and Alessina developed the matrix converter, presenting the power circuit of a converter as a matrix of bidirectional power switches [12]. Meanwhile, the interest in this technology has been growing with the technological development that has allowed to create zones of operation at high frequencies and, at the same time, relatively low driving voltage drops [11, 13].

This technology stands out from the rest due to its several advantages, such as allowing a bidirectional power flow and presenting a high efficiency, which can reach 98% [11, 14]. Moreover, in contrast to other converters, it provides a reduction in volume and cost since it does not have an intermediate DC link, it does not need to have DC bulky electrolytic capacitors [11, 13].

Figure 4a shows the model to be used in the system matrix converters, a single-phase matrix converter formed by four bidirectional switches. Theoretically, this type of converters should allow 2^4 connection combinations [13]. However, it is necessary to consider the restrictions of the typology, that is, voltage sources should not be short-circuited, and current sources should not be left open [12, 13]. Consequently, this system only has four possible combinations [13].

Moreover, figure 4b presents the architecture defined for the switches, the common-emitter antiparallel Insulated Gate Bipolar Transistor (IGBT), diode pair. In this way, the diode provides the switching module the reverse blocking capability, while the IGBT guarantees high-frequency switching capabilities [14].

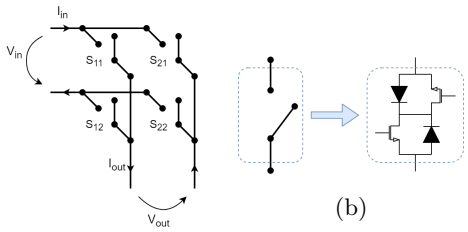

(a) (b)

Figure 4: (a) Graphical representation of a single-phase MC (adapted from [11]); (b) Graphical representation of a bi-directional switch module (adapted from [11]).

Each bidirectional switch can be mathematically defined by a variable S_{kj}, assuming ideal semiconductors, which can assume two possible states: "$S_{kj} = 1$" if the switch is ON and "$S_{kj} = 0$" if the switch is OFF, as presented in the expression (1)[11, 13].

$$S_{kj} = \begin{cases} 1 & \text{, if switch is ON } \ k \in \{1, ..., m\} \\ 0 & \text{, if switch is OFF } j \in \{1, ..., n\} \end{cases} \quad (1)$$

Therefore, and considering that the system converters have a current source based conversion system, the possible switching states are those shown in table 1.

	State	S_{11}	S_{12}	S_{21}	S_{22}	V_{out}
1	1	1	0	0	1	V_{in}
2	-1	0	1	1	0	$-V_{in}$
3	0	1	1	0	0	0
4	0	0	0	1	1	0

Table 1: Matrix converters's switching states.

As previously mentioned, the proposed solution contains two matrix converters. However, they perform different functions in the system, so the switching strategy for each one is different. Next, the strategies chosen for each case are presented.

2.2.1 AC/AC Matrix Converter Switching Strategy

The goal of the AC/AC matrix converter is to convert a sinusoidal sign with a frequency of 50 Hz into another signal with the same amplitude but switched at 50 kHz. Therefore, the switching strategy to be applied is the full-wave command.

The full-wave command is a two-level command, where the switch pairs S_{11}, S_{22}, and S_{12}, S_{21} are commanded in a complementary manner [13]. That is, during $T_s/2$, the switches S_{11} and S_{22} are commanded to drive, while S_{12} and S_{21} are commanded to cut-off. And, during the other half-period, S_{12} and S_{21} are set to drive, while S_{11} and S_{22} are set to cut-off [13].

2.2.2 AC/DC Matrix Converter Switching Strategy

The AC/DC matrix converter aims to convert the current on the secondary side of the HFT into a synchronous, rectified sinusoidal current with the AC network. Although using the full-wave command as a switching strategy is not enough because it is crucial to recover the signal from the AC network voltage to have a bidirectional flow.

Consequently, it is necessary to apply a modified full-wave command. So, during T /2, the command signal is the same as described in the previous section and used in the AC/AC MC, whereas in the other half-period, the command signal is the symmetric of the previous one.

2.3. Step-Up Converter

The step-up converter, also known as a boost converter, is a type of DC/DC power converter, which allows raising the input voltage. Figure 5 shows the diagram of the model of the converter to be used.

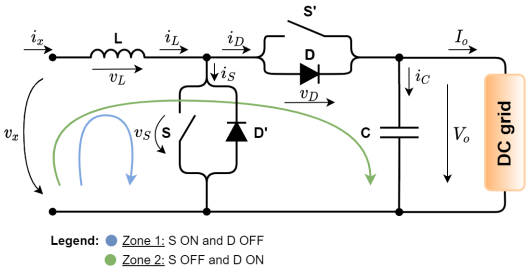

Figure 5: Diagram of the boost converter (adapted from [15]).

Considering a steady-state operation and the Continuous Conduction Mode (CCM), the average value of the voltage in inductance is zero ($v_{L\,av} = 0$), and it is possible to calculate a relationship between the input and output voltages present in the expression (2) [15].

$$\frac{V_o}{v_x} = \frac{1}{1-\delta} \Leftrightarrow v_x = (1-\delta)V_o \quad (2)$$

2.3.1 Sizing of L

Assuming the differential equation that describes the progress of the current in L and linearizing the variation of the current, we obtain the expression (3).

$$v_L = L\frac{d\,i_L}{d\,t} \Rightarrow \frac{\Delta i_L}{\Delta t} = \frac{v_L}{L} \quad (3)$$

When S is ON, it is possible to consider $v_L = v_x$, and $\Delta t = \delta T_s$, and this way, define the value of

the inductor current ripple, Δi_L. By setting the Δi_L value, it is possible to dimension L through the expression (4).

$$\Delta i_L = \frac{v_x}{L}\,\delta T_s \Rightarrow L = \frac{V_o(1-\delta)\delta T_s}{\Delta i_L} \tag{4}$$

However, the expression (4) can be simplified by expression (5) when V_o is constant, and this is the expression used to size L.

$$if\ V_o = const\ \Rightarrow\ L_{max} = \frac{V_o\,T_s}{4\Delta i_L}\ when\ \delta = \frac{1}{2} \tag{5}$$

2.3.2 Sizing of C

Similar to the current of the i_L, the voltage variation of the capacitor can also be linearized, which is defined by the expression (6).

$$i_C = C\,\frac{d\,u_C}{d\,t} \Rightarrow \frac{\Delta V_o}{\Delta t} = \frac{i_C}{C} \tag{6}$$

Furthermore, ΔV_o can also be described by expression (7).

$$\Delta V_o = \frac{\Delta Q}{C} = \frac{1}{wC}\int_{\frac{3\pi}{4}}^{\frac{5\pi}{4}} i_C(wt)\,d\,wt \tag{7}$$

Performing a mathematical analysis of the system and neglecting the losses of the converter, it is possible to define the i_C and i_L currents based on the AC and DC network power. From these deductions, it is possible to rewrite expression (7) by expression (8).

$$\Delta V_o = \frac{I_o}{2\,w\,C}[sin(2wt)]_{\frac{3\pi}{4}}^{\frac{5\pi}{4}} = \frac{I_o}{w\,C} \tag{8}$$

Finally, the expression (9) is obtained, which allows us to size the capacitor C by setting the value of the V_o voltage ripple, ΔV_o.

$$C = \frac{I_o}{w\,\Delta V_o} = \frac{P_o}{w\,V_o\,\Delta V_o} \tag{9}$$

2.4. Constant Power Load

Controlling a DC network presents several challenges, one of the most important being the requirements of the power electronic loads [2]. In general, these loads behave as Constant Power Loads (CPL) because, they absorb a constant power, i.e., $dP_{cpl} = 0$ in steady-state [2, 16]. Since dP_{cpl} is equal to zero, it is possible to derive (10) and to conclude that, as a result of the power being constant, the load may be represented as a the negative incremental resistance, r_i [2].

$$\begin{gathered} dP_{cpl} = V_{o_{cpl}}\,dI_{o_{cpl}} + I_{o_{cpl}}\,dV_{o_{cpl}} = 0 \Leftrightarrow \\ \Leftrightarrow {}^{dV_{o_{cpl}}}/_{dI_{o_{cpl}}} = -{}^{V_{o_{cpl}}}/_{I_{o_{cpl}}} = r_i \end{gathered} \tag{10}$$

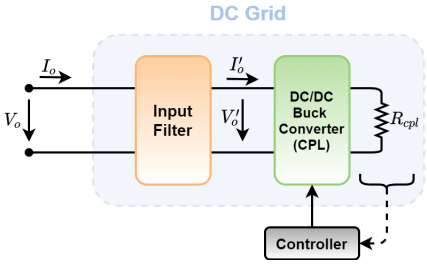

Figure 6: DC grid and Constant Power Load configurations.

By analyzing the relation present in expression (10), it is possible to verify that if the voltage at the CPL input decreases then the current at its input increases. Therefore, the presence of CPL can cause a decrease of the equivalent resistance of the system, oscillations in the system voltages and currents and may also lead to voltage collapse [16].

A CPL load can have several topologies, although, in this paper, the CPL consists of a buck converter with an input filter, as shown in figure 6. Besides, the CPL has its control system, which is explained in section 3.

2.4.1 Step-Down Converter

Step down converters,also known as buck converters, are used whenever it is necessary to reduce a given DC voltage to a lower value [17]. The step-down converter can be implemented by the circuit present in figure 7 [18].

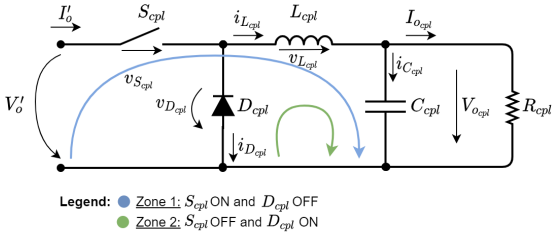

Figure 7: Diagram of the buck converter (adapted from [18]).

Considering the operation in the steady-state and the CCM operating mode, it is possible to assume the relation between V'_o and $V_{o_{cpl}}$ stated in expression (11).

$$\frac{V_{o_{cpl}}}{V'_o} = \delta \Leftrightarrow V_{o_{cpl}} = V'_o\,\delta \tag{11}$$

The next step consists of sizing the elements of the converter. In the case of L_{cpl}, the procedure is similar to the one used in the boost converter, in section 2.3.1. Therefore, expression (12) presents the formula used to size L_{cpl}.

$$if\ V_{o_{cpl}} = const \Rightarrow$$
$$L_{cpl\,max} = \frac{V_{o_{cpl}}\,T_s}{\Delta i_{L_{cpl}}}\ when\ \delta = 0 \tag{12}$$

To size the C_{cpl}, it is considered that it is almost constant and that $\Delta V_{o_{cpl}} \ll V_{o_{cpl}}$, and then the variation of the load, ΔQ, is defined. After several algebraic manipulations, it is possible to derive C_{cpl} through (13), and for this, it is necessary to fix the value of the $V_{o_{cpl}}$ voltage ripple, $\Delta V_{o_{cpl}}$.

$$if\ V_{o_{cpl}} = const\ \Rightarrow$$
$$C_{cpl\,max} = \frac{V_{o_{cpl}}\,{T_s}^2}{8\,L_{cpl}\Delta V_{o_{cpl}}}\ when\ \delta = 0 \tag{13}$$

Figure 8 shows the input filter scheme to be implemented before the CPL to reduce system disturbances and oscillations [19].

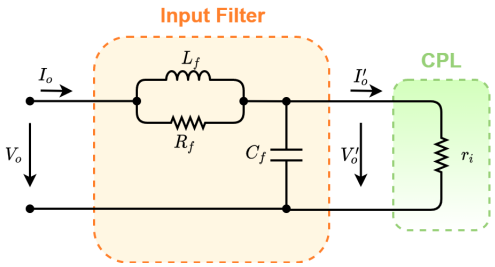

Figure 8: Diagram of the input filter (adapted from [19]).

Nevertheless, to achieve the objectives, it is necessary to size the filter correctly. Therefore, the first step consists of defining the transfer function of the system, presented in expression (14) [19].

$$\frac{V'_o(s)}{V_o(s)} = \frac{\frac{1}{C_f L_f}\left(s\frac{L_f}{R_f}+1\right)}{s^2 + s\frac{\sqrt{\frac{L_f}{C_f}}}{\left(\frac{R_f r_i}{R_f+r_i}\right)}\sqrt{\frac{1}{C_f L_f}} + \frac{1}{C_f L_f}} \tag{14}$$

To minimize the influence of the transfer function zero, the real zero $-\frac{R_f}{L_f}$ should be placed to the left and as far as possible from the real part of the conjugated pole, $-\zeta w_c$ [19]. In this way, expression (15), which relates R_f to the characteristic impedance of the LC filter, $Z_f = \sqrt{L_f/C_f}$, is deduced [19]. H_f is a positive constant greater than or equal to 1.

$$-\frac{R_f}{L_f} < -\zeta w_c \Leftrightarrow R_f > \zeta Z_f \Rightarrow R_f = H_f \zeta Z_f \tag{15}$$

After some algebraic manipulations and once the stability of Routh-Hurwitz is guaranteed, it is possible to define R_f by expression (16) [19].

$$R_f \approx \frac{Z_f}{2\zeta},\quad Z_f \ll |\ 2\zeta r_i\ | \tag{16}$$

On the other hand, Z_f can be defined by expression (17), assuming that H_f is equal to $1/3\zeta^2$ [19].

$$Z_f = -\zeta r_i \tag{17}$$

Regarding the cut-off frequency, f_c, it must be at least one decade above the AC grid frequency, f, and one decade below the switching frequency, f_s [11]. Moreover, the value of the damping factor, ζ, must be between 0.5 and 0.7 [19]. In fact, f_c should be a decade above the double of the AC grid frequency, because during the conversion process the voltage is rectified. Finally, the L_c and C_f elements can be sized by the definition of Z_f, as the f_c and Z_f values have already been previously established.

3. Control System Design

For the system to work duly, it must be ensured that it is suitably controlled. The control system proposed in this paper is a non-linear system and includes two controllers with two loops. The outer loop is the voltage controller, which is based on the backstepping theory and defines the reference for the current i_L, $I_{L\,ref}$. On the other hand, the inner loop refers to the current controller, which is based on Sliding Mode Controller.

3.1. Backstepping Voltage Controller

The goal is to guarantee $V_o = V_{o\,ref}$. Therefore, the first step consists of defining the V_o voltage error, e_{V_o}, as the difference between the reference signal, $V_{o\,ref}$, and the measured voltage V_o, $(e_{V_o} = V_{o\,ref} - V_o)$. To ensure e_{V_o} to be zero, the Lyapunov function, V_1, in (18), is proposed.

$$V_1(e_{V_o}) = \frac{1}{2}{e_{V_o}}^2 + K_I\,\frac{{e_I}^2}{2},\ K_I > 0 \tag{18}$$

Where K_I is a chosen positive constant, and e_I represents the integral error, $\left(e_I = \int_0^t e_{V_o}\,dt = 0\right)$. With this integral component it is possible to guarantee a zero static error.

Since, expression (18) is a Lyapunov's function, the following restrictions must be fulfilled: i) $V_1(e_{V_o} = 0) = 0$; ii) $V_1(e_{V_o} \neq 0) > 0$; iii) $V_1(|e_{V_o}| \to \infty) \to \infty$; iv) $\dot{V}_1(e_{V_o} \neq 0) < 0$ [20].

Regarding the stability condition $\left(V_1(e_{V_o} \neq 0) \cdot \dot{V}_1(e_{V_o} \neq 0) < 0\right)$, the Lyapunov second method global asymptotic stability is given by expression (19) [2].

$$\dot{V}_1 = e_{V_o}\,\dot{e_{V_o}} + K_I\,e_I\,e_{V_o} < 0 \tag{19}$$

The expression (20) provides a new definition of $\dot{V}_1$ to ensure the condition indicated in the expression (19).

$$\dot{V}_1 = -K_v \, {e_{V_o}}^2, \qquad K_v > 0 \tag{20}$$

By considering the diagram in figure 5 and the previous definitions of e_{V_o} and $e\dot{V}_o$, it is possible to deduce expression (21).

$$\dot{e}_{V_o} = \dot{V}_{o\,ref} - \frac{i_L - I_o}{C} = -K_v \, e_{V_o} - K_I \, e_I \tag{21}$$

By replacing i_L with $i_{L\,ref}$ in expression (21), it is possible to obtain the new reference value for the current present in expression (22). This expression does not include the term referring to the $V_{o\,ref}$ time derivative since this is the reference voltage of the DC grid voltage, and its time derivative is null.

$$i_{L\,ref} = C \left(K_v \, e_{V_o} + K_I \, e_I \right) + I_o \tag{22}$$

From (22), it can be seen that the reference value for the current depends on the error of the voltage.

Remembering that the desired waveform for the i_L current is a rectified sinusoid and synchronous with the AC grid, it turns out that the previous control law is not enough to provide the desired wave. Therefore, the proposed solution consists of multiplying the reference value obtained by the expression (22) by a rectified sinusoid, with maximum unitary amplitude and synchronous with the AC network.

3.2. Sliding Mode Current Controller

The next step in the control system development consists of setting the non-linear current controller. The proposed solution consists of controlling the semiconductor S through the signal coming from a hysteresis comparator. Therefore, expression (23) describes the operation of the boost converter.

$$\gamma = \begin{cases} 1 & \text{if } S\,\text{ON} \quad \text{then, } v_L = v_x \\ 0 & \text{if } S\,\text{OFF} \quad \text{then, } v_L = v_x - V_o \end{cases} \tag{23}$$

The goal is to guarantee $i_L = i_{L\,ref}$, so the i_L current error, e_{i_L}, can be defined as the difference between the reference signal, $i_{L\,ref}$, and the measured i_L current ($e_{i_L} = i_{L\,ref} - i_L$). Besides, e_{i_L} is also defined as the linear surface variable in time, $s(x)$, thus being possible to apply the sliding mode controller [21].

Considering $v_L = L\frac{d\,i_L}{dt}$ and remembering that $V_o > v_x$, it is possible to deduct the expression (24).

$$\begin{cases} v_L = v_x & \Rightarrow \quad {}^{d\,i_L}/_{dt} > 0 \\ v_L = v_x - V_o & \Rightarrow \quad {}^{d\,i_L}/_{dt} < 0 \end{cases} \tag{24}$$

To ensure stability, the function $s(x)$ must guarantee the sliding mode stabilitycondition, $s(x)\,\dot{s}(x) < 0$ [22]. Therefore, it is possible to infer the relations present in expression (25).

$$\begin{cases} \text{if } e_{i_L} > 0 \Rightarrow \frac{d\,e_{i_L}}{dt} < 0 \Rightarrow \frac{d\,i_L}{dt} > \frac{d\,i_{L\,ref}}{dt} \\ \text{if } e_{i_L} < 0 \Rightarrow \frac{d\,e_{i_L}}{dt} > 0 \Rightarrow \frac{d\,i_L}{dt} < \frac{d\,i_{L\,ref}}{dt} \end{cases} \tag{25}$$

However, the expression (25) need to be adapted to make the system physically feasible. Therefore, the new purpose of the controller is to ensure that the error is within a boundary layer, $-\Delta/2 < e_{i_L} < \Delta/2$ [21, 22]. So, the expression (25) is replaced by the expressions (26) and (27).

$$\begin{gathered} \text{if } e_{i_L} > +\tfrac{\Delta}{2} \Rightarrow i_L < i_{L\,ref} \\ \text{then, } i_L \nearrow \Rightarrow \tfrac{d\,i_L}{dt} > 0 \Rightarrow S\,\text{ON}\,(\gamma = 1) \end{gathered} \tag{26}$$

$$\begin{gathered} \text{if } e_{i_L} < -\tfrac{\Delta}{2} \Rightarrow i_L > i_{L\,ref} \\ \text{then, } i_L \searrow \Rightarrow \tfrac{d\,i_L}{dt} < 0 \Rightarrow S\ \text{OFF}(\gamma = 0) \end{gathered} \tag{27}$$

Finally, figure 9 shows the diagram of the proposed control system, where it presents all the elements mentioned above.

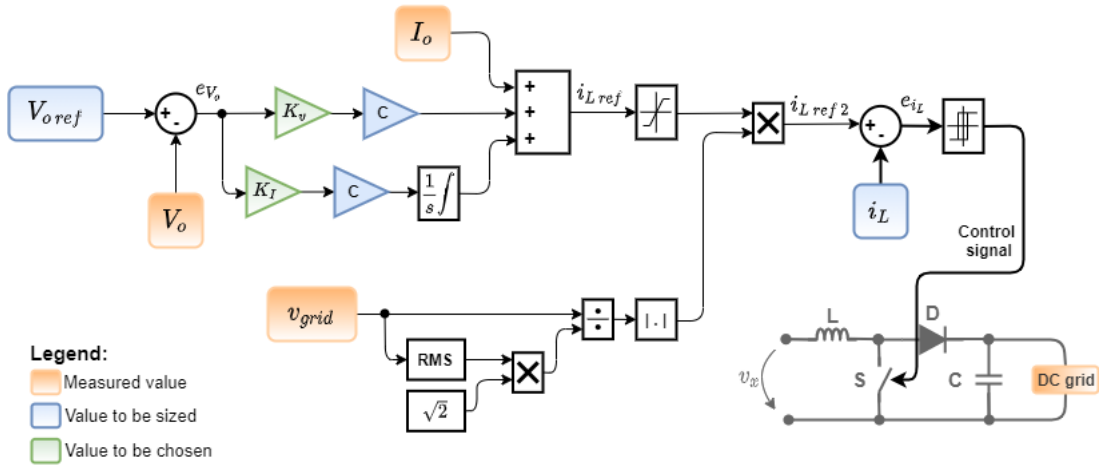

Figure 9: Block diagram of the control system.

3.3. Constant Power Load Control System

To control the CPL, the choice is identical to the previous case, so the deduction from the control laws is very similar to the one made previously. Therefore, this paper only presents the final control laws. Expression (28) introduces the intermediate control law, which defines the reference of the $i_{L_{cp}}$ current, and expressions (29) and (30) include the control law to the S_{cpl} semiconductor.

$$i_{L_{cpl\,ref}} = C_{cpl}\left(K_v \dot{e}_{V_{o_{cpl}}} + K_I e_{I_{cpl}} + \dot{e}_{V_{o_{cpl}}}\right) + I_{o_{cpl}} \tag{28}$$

$$\begin{aligned} &\text{if } e_{i_{L_{cpl}}} > +\tfrac{\Delta}{2} \Rightarrow i_{L_{cpl}} < i_{L_{cpl\,ref}} \text{ then,} \\ &i_{L_{cpl}} \nearrow \Rightarrow \tfrac{d\,i_{L_{cpl}}}{dt} > 0 \Rightarrow S_{cpl}\,\text{ON}\,(\gamma = 1) \end{aligned} \tag{29}$$

$$\begin{aligned} &\text{if } e_{i_{L_{cpl}}} < -\tfrac{\Delta}{2} \Rightarrow i_{L_{cpl}} > i_{L_{cpl\,ref}} \text{ then,} \\ &i_{L_{cpl}} \searrow \Rightarrow \tfrac{d\,i_{L_{cpl}}}{dt} < 0 \Rightarrow S_{cpl}\,\text{OFF}(\gamma = 0) \end{aligned} \tag{30}$$

4. Simulation Results

This new chapter presents the parameter values and the results obtained in the simulation of different operation scenarios to analyze the system behavior. The cases considered in simulation differ from each other by the operating conditions of the DC grid, and all the simulations were performed using Matlab's Simulink tool.

4.1. Simulation Parameters

Table 2 shows the parameters of all the system elements used in the different scenarios. The data from the CPL refer to the third case study.

Table 2: Simulation parameters of the all system elements.

AC Grid	V_{rms}	230	V	**DC Grid**		$V_{o\,ref}$	400	V
	f	50	Hz			P_o	2	kW
HFT	f_s	50	kHz	**CPL**	**Input Filter**	f_c	1	kHz
	V_p	230	V			ζ	0.6	
	V_s	230	V			R_f	45	Ω
	P_n	2	kVA			L_f	8.594	mH
	R_{T1}, R_{T2}	0.106	Ω			C_f	2.947	μF
	L_{T1}, L_{T2}	1.587	μH		**Buck Converter**	$\Delta i_{L_{cpl}}$	10%	$i_{L_{cpl}}$
	R_m	5.290	MΩ			$\Delta V_{o_{cpl}}$	1%	$V_{o_{cpl}}$
	L_m	2.846	H			L_{cpl}	18.0	mH
Boost Converter	Δi_L	10%	i_L			C_{cpl}	0.278	mF
	ΔV_o	1%	V_o			R_{cpl}	80	Ω
	L	2.3	mH					
	C	3.979	mF					

Regarding the control system, it is necessary to set the values for K_v and K_I gains so that it is possible to incorporate the control system in the simulation. However, the only restriction imposed on these gains so far is that they both must be positive constants.

After performing several tests with different values of K_v and K_I, the best values are K_v equals 80 and K_I equals $20e^3$, being these the values used in the simulation.

4.2. Study Scenarios

This section presents the main results obtained in the four scenarios considered.

4.2.1 DC Grid with a Single Resistive Load

In this study case, the DC grid is represented only by a resistive load equal to 80 Ω. The main results are represented in figure 10, where figure 10a includes the AC grid results and the figure 10b includes the DC grid results.

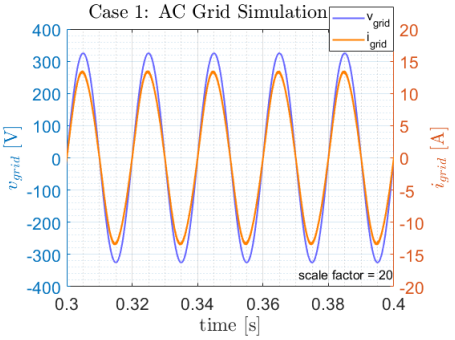

(a) AC grid: v_{grid} in blue and i_{grid} in orange.

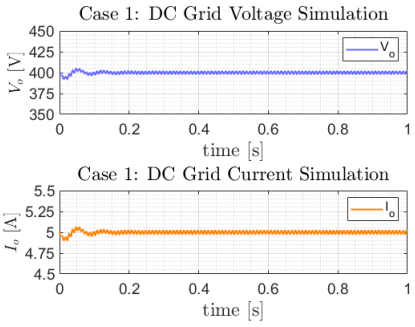

(b) DC grid: V_o in blue and I_o in orange.

Figure 10: Simulation results in case 1.

By analyzing the graphs, it appears that the results are in line with expectations. In the case of the AC grid, voltage and current are in phase, and they have a sinusoidal waveform, as desired. On the other hand, the DC grid results indicate that voltage V_o is approximately constant and follows its reference value, which is equal to 400 V. As already mentioned in section 2.3.2, the V_o voltage always presents a small ripple due to the high-frequency switching. However, this ripple does not exceed the value set in table 2, so the conclusion is that it has

an acceptable value, and it confirms that the results are as expected.

4.2.2 DC Grid with Two Resistive Loads in Parallel

The second case presents the DC grid characterized by two resistive loads in parallel (R_1 and R_2), both equal to 160 Ω. The simulation starts only with R_1 connected, and only at time instant, t_1 (0.5 s), load R_2 is connected. The results for the AC grid and the DC grid are shown in figures 11a and 11b, respectively.

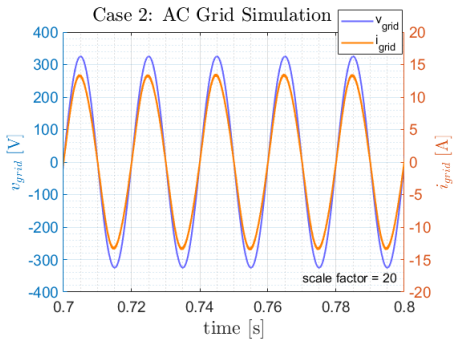

(a) AC grid: v_{grid} in blue and i_{grid} in orange.

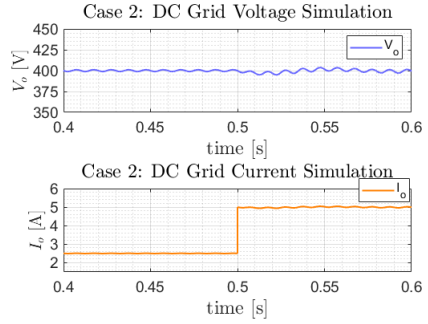

(b) DC grid: V_o in blue and I_o in orange.

Figure 11: Simulation results in case 2.

After the second load is connected, the current values increase, as expected. From this moment on, the system goes through a short transient before reaching the steady-state, observed in figure 11a, where it is visible that the current and voltage have the intended sinusoidal waveform.

Once again, the DC voltage presents a small ripple, which does not exceed the value established in table 2. Therefore, the system provides the desired response.

4.3. DC Grid with a Constant Power Load

In this scenario, the DC network only has a CPL with an input filter, as in figure 6, and, as in the previous cases, figure 12 presents the simulation results of the AC and DC grids.

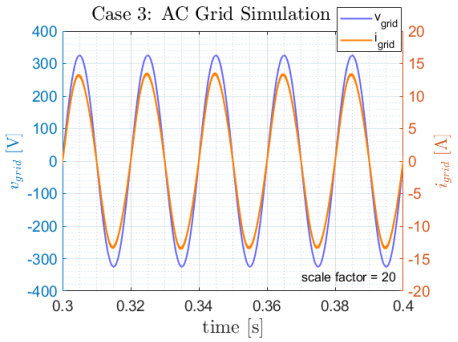

(a) AC grid: v_{grid} in blue and i_{grid} in orange.

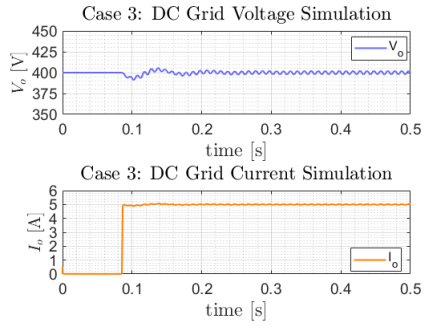

(b) DC grid: V_o in blue and I_o in orange.

Figure 12: Simulation results in case 3.

Analyzing the figure 12, we conclude that the system continues to work correctly even with a more complex configuration of the DC network. That means that after the initial transient period, it is verified that on the AC side, the waveforms are sinusoidal, and on the DC side, the waveforms are approximately constant. Therefore, the signals to be controlled successfully follow their references, including the signals from the CPL control system.

4.4. DC Grid with a Current Source

The last study scenario aims to show one of the main characteristics of the system already mentioned, the bidirectional power flow, that may result from the connection of a renewable power source, as a photovoltaic (PV) system, to the DC grid. In this way, a current source is added to the DC network to observe the change in the direction of the current, compared to the previous cases. Therefore, the DC grid now consists of a parallel current source with a resistive load, R_o, where R_o is equal to 80 Ω, and the current source, I_{DC} is defined with a value equal to $2I_o$, i.e., 10 A.

As in the previous cases, the simulation results of both networks are presented below in figure 13.

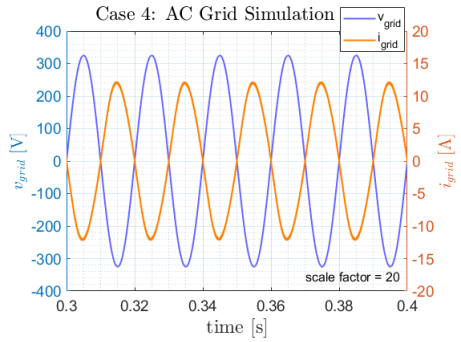

(a) AC grid: v_{grid} in blue and i_{grid} in orange.

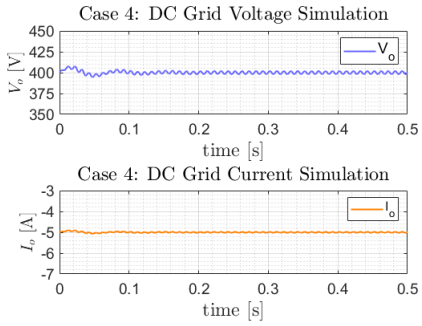

(b) DC grid: V_o in blue and I_o in orange.

Figure 13: Simulation results in case 4.

Analyzing figure 13, it is clear that the new results are different from previous ones. In this case, the voltage and current of the AC grid continue to present sinusoidal waveforms but are no longer in phase. They are now out of phase, which indicates that the current has changed direction. Therefore, it has been possible to show that the system allows bidirectional power flow.

DC network results are another indicator that the system is bidirectional. Because although both signals are approximately constant, it is verified that the current has a negative value, meaning that the current flows in the opposite direction compared to the other scenarios.

5. Conclusions

This article focuses on the study of a single-phase, bi-directional, and isolated AC/DC converter that allows connecting a low voltage AC grid to a DC grid. In this way, it is possible to create a hybrid network, that when compared to the existing AC network, allows reducing the number of conversions and consequently increase the overall efficiency of the system and reduce its losses.

After a detailed study of the proposed system, the components of the various elements are sized, and the command signals of the matrix converters are defined, considering the role each one has in the system.

A non-linear control system is developed to ensure that the conversion system does not create disturbances in the AC and DC networks. This controller is based on the backstepping and sliding mode control theories.

Through the analysis of the results of the simulations, we realize that the proposed solution presents an adequate response in different scenarios. The conclusions reached in the first three cases are identical and confirm that the system meets the requirements imposed on it. This means that both the voltage and the current of the AC grid present sinusoidal waveforms and without disturbances, as was desired. On the other hand, the current and voltage of the DC grid have approximately constant waveforms, and there is a small ripple considered acceptable. The last scenario has a specific objective, to show that the system is bidirectional and the results prove that.

Although the proposed system achieves all the proposed objectives, this system can still be improved. Therefore, it is suggested that for future research, it would be interesting to develop a model more complex and closer to reality. An another improvement would be to build a prototype in the laboratory and therefore conduct a more reliable evaluation of the system. Finally, it is suggested that an economic evaluation of the proposed solution be conducted because besides having a system that presents successful results, the project must be economically viable.

Acknowledgements

I would like to thank the project of the Fundação para a Ciência e a Tecnologia (FCT) PTDC/EEI-EEE/32550/2017 - Smart Transformers for Sustainable Grids, since it was within this project that the opportunity appeared to develop the topic of this paper.

References

[1] Wang, P., et al. Harmonizing AC and DC: A hybrid AC/DC future grid solution. *IEEE Power and Energy Magazine*, 2013, 11.3: 76-83.

[2] Paraíso, G. M.; Pinto, S. F.; Silva, J. F. Modelling and nonlinear control of Dual-Active Bridge converters for DC microgrids. In: IECON 2019-45th *Annual Conference of the IEEE Industrial Electronics Society*. IEEE, 2019. p. 1850-1855.

[3] Liu, X.; Wang, P.; Loh, P. C. A hybrid AC/DC microgrid and its coordination control. *IEEE Transactions on smart grid*, 2011, 2.2: 278-286.

[4] Flaticon, available online: www.flaticon.com (last acess: 30.10.2020)

[5] Everts, J. Modeling and optimization of bidirectional dual active bridge ac-dc converter topolo-

gies. *ARENBERG DOCTORAL SCHOOL FACULTY OF ENGINEERING SCIENCE,* 2014.

[6] Van der Merwe, J. W.; Mouton, H. du T. The solid-state transformer concept: A new era in power distribution. In: *AFRICON 2009.* IEEE, 2009. p. 1-6.

[7] Gonzalez-Garcia, C.; Pleite, J. Transformer model in wide frequency bandwidth for power electronics systems. *Advances in Power Electronics*, 2013, 2013.

[8] She, X.; Huang, A. Q.; Burgos, R. Review of solid-state transformer technologies and their application in power distribution systems. *IEEE journal of emerging and selected topics in power electronics*, 2013, 1.3: 186-198.

[9] Bhattacharya, S., et al. Design and development of generation-I silicon based solid state transformer. In: *2010 Twenty-Fifth Annual IEEE Applied Power Electronics Conference and Exposition (APEC)*. IEEE, 2010. p. 1666-1673.

[10] Fan, H.; Li, H. High-frequency transformer isolated bidirectional DC–DC converter modules with high efficiency over wide load range for 20 kVA solid-state transformer. *IEEE Transactions on Power Electronics*, 2011, 26.12: 3599-3608.

[11] Pinto, S. F.; Mendes, P. V.; Silva, J. F. Modular matrix converter based solid state transformer for smart grids. *Electric Power Systems Research*, 2016, 136: 189-200.

[12] Wheeler, P. W., et al. Matrix converters: A technology review. *IEEE Transactions on industrial electronics,* 2002, 49.2: 276-288.

[13] Silva, J. F.; Pinto, S.; Santana, J. Conversores Comutados para Energias Renováveis. *Support text, IST*, 2013.

[14] Idris, Z.; Noor, SZ M.; Hamzah, M. K. Safe commutation strategy in single phase matrix converter. In: *2005 International Conference on Power Electronics and Drives Systems*. IEEE, 2005. p. 886-891.

[15] Hasaneen, B. M.; Mohammed, A. A. E. Design and simulation of DC/DC boost converter. In: *2008 12th International Middle-East Power System Conference*. IEEE, 2008. p. 335-340.

[16] Singh, S.; Gautam, A. R.; Fulwani, D. Constant power loads and their effects in DC distributed power systems: A review. *Renewable and Sustainable Energy Reviews*, 2017, 72: 407-421.

[17] Di Bernardo, M.; Budd, C.; Champneys, A. Grazing, skipping and sliding: analysis of the non-smooth dynamics of the DC/DC buck converter. Nonlinearity, 1998, 11.4: 859.

[18] Wei, X.; Tsang, K. M.; Chan, W. L. DC/DC buck converter using internal model control. *Electric Power Components and Systems*, 2009, 37.3: 320-330.

[19] Silva, J. F. Input filter design for power converters. In: *Lecture notes*. IST, 2012.

[20] Kalman, R. E.; Bertram, J. E. Control system analysis and design via the "second method" of Lyapunov: I—continuous-time systems. 1960.

[21] Utkin, V. I. Sliding mode control design principles and applications to electric drives. *IEEE transactions on industrial electronics*, 1993, 40.1: 23-36.

[22] Da Silva, J. F. A., et al. Advanced control methods for power electronics systems. *Mathematics and computers in simulation*, 2003, 63.3-5: 281-295.